

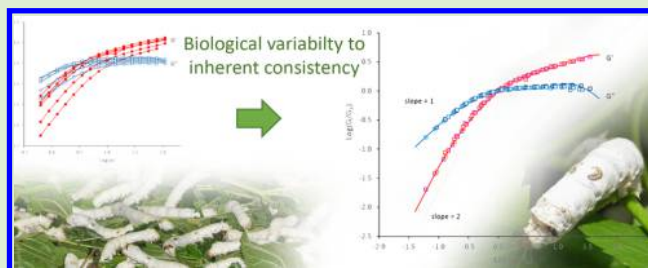


Native Silk Feedstock as a Model Biopolymer: A Rheological Perspective

Peter R. Laity* and Chris Holland*

Department of Materials Science and Engineering, The University of Sheffield, Sir Robert Hadfield Building, Mappin Street, Sheffield, S1 3JD, United Kingdom

ABSTRACT: Variability in silk's rheology is often regarded as an impediment to understanding or successfully copying the natural spinning process. We have previously reported such variability in unspun native silk extracted straight from the gland of the domesticated silkworm *Bombyx mori* and discounted classical explanations such as differences in molecular weight and concentration. We now report that variability in oscillatory measurements can be reduced onto a simple master-curve through normalizing with respect to the crossover. This remarkable result suggests that differences between silk feedstocks are rheologically simple and not as complex as originally thought. By comparison, solutions of poly(ethylene-oxide) and hydroxypropyl-methyl-cellulose showed similar normalization behavior; however, the resulting curves were broader than for silk, suggesting greater polydispersity in the (semi)synthetic materials. Thus, we conclude Nature may in fact produce polymer feedstocks that are more consistent than typical man-made counterparts as a model for future rheological investigations.



INTRODUCTION

Silks are protein fibers produced by many types of arthropods.^{1,2} Those produced by spiders and some lepidopteran larvae (i.e., caterpillars) are well-known and have been researched extensively,^{2–8} while the silks produced by other insects^{9–11} and myriapods (i.e., centipedes and millipedes)^{12,13} have received much less attention. The fibers from different species have different protein compositions, serve a wide range of uses, and may be produced from different glands, suggesting multiple cases of convergent evolution.¹⁰ Nevertheless, in spite of this diversity, the fibers are all produced in a similar way: an aqueous protein feedstock is synthesized and stored in special glands inside the body, then extruded “on demand” at relatively high speeds (from around 4 mm s⁻¹ for silkworm cocoon fibers, up to 500 mm s⁻¹ for forcibly spun spider dragline¹⁴). This distinguishes silk from other animal fibers, such as hair, which grow continuously but at much slower rates (e.g., around 0.3–0.4 mm day⁻¹ for sheep's wool¹⁵).

Natural silk spinning occurs by extruding an aqueous medium at body temperature (i.e., essentially ambient temperature for ectothermic animals) through a spinneret and formation of a solid fiber is believed to occur by a flow-induced phase transition.^{8,14,16,17} The relatively mild conditions under which this occurs are in stark contrast to industrial fiber spinning, which typically involves esoteric or harmful process chemicals (for wet or dry spinning) or high temperatures (for melt spinning),^{18,19} in order to engineer sufficiently large changes in physical conditions or chemical composition to drive solidification and stabilize the nascent fibers. Hence, one may expect that fiber production methods similar to the natural

spinning of silks could offer very large energy savings over conventional industrial methods.²⁰

It is widely accepted that flow behavior is an important factor in the natural fiber spinning process. Consequently, there have been numerous studies into the rheology of native silk feedstocks from various species of silkworms and spiders.^{21–29} In spite of the different origins of the materials, these works generally revealed non-Newtonian rheological behavior typical of concentrated polymer solutions, including shear thinning above a threshold rate of steady flow and viscoelastic responses to oscillatory measurements.

Recent work on native silk protein feedstocks from the domesticated silk worm (*Bombyx mori*) confirmed surprisingly large sample-to-sample variations, in spite of using nominally similar materials (i.e., solutions containing predominantly fibroin protein) from the same section (middle posterior division) of the silk glands, which were excised at a similar developmental stage (5th instar, during early stage of cocoon construction).²¹ Several potential explanations for this were explored: a weak correlation was observed with the protein concentration, while the possibility of some small variability in protein molecular weight has been reported previously.^{30,31} Nevertheless, neither appeared sufficient to explain the range of viscosities observed.

The present work examines this variability in greater detail. Rather than random differences, however, clear relationships are demonstrated between key rheological characteristics,

Received: May 16, 2016

Revised: June 17, 2016



including the shear viscosity, the location of the crossover between solid- and liquid-like viscoelastic behavior and the values of the various parameters obtained by fitting the oscillatory data using a “Maxwell-type” model. These relationships suggest that the observed rheological variability is not merely adventitious, but is probably caused by systematic changes in the silk protein feedstock in the gland, which are expected to be under biological control within the silkworm.

The work culminated in a rather striking observation: oscillatory data from native silk feedstock specimens with widely divergent viscosities can be “normalized” using their crossover point. When combined, the results showed a remarkably good superposition, generating master-curves for the elastic and viscous moduli, which effectively extended the observable angular frequency range. This facilitated successful curve-fitting using a three term Maxwellian model, which provided a more detailed picture of the rheology.

EXPERIMENTAL SECTION

Native silk feedstock specimens were obtained from fifth instar *B. mori* larvae during early stages of cocoon construction and characterized using methods similar to those described previously.²¹ In summary, silk glands were excised and the epithelial membrane was peeled off under cold (ca. 5 °C) distilled water, using fine tweezers and a dissection microscope. A portion (ca. 0.01–0.02 g) of the (predominantly) fibroin solution from the middle posterior section of the gland was carefully transferred to a rheometer (Bohlin Gemini, Malvern Instruments Ltd. Malvern, U.K.), fitted with a Peltier heating and cooling stage and a CP1/10 geometry (10 mm diameter cone with 1° opening angle and 30 μm truncation). Excess water was removed from the surface of the specimen, by absorbing it into a small piece of tissue paper, before lowering the cone. The closing speed was reduced to the slowest (ca. 0.1 mm s⁻¹), to minimize the associated (shear and extensional) flow. The small amount of excess material around the cone was not removed, to avoid any risk of flow-induced gelation. The entire sample area was flooded with distilled water, then enclosed within a loosely fitting cover to prevent drying and skin formation.

At the same time, a larger portion (0.1–0.2 g) of the native silk feedstock from the adjacent segment of gland was also removed and used to determine the concentration of solid residue after drying to constant weight under vacuum at 60 °C.

The rheometer was controlled using the Bohlin software, which also performed the initial data processing. Rheological behavior of each specimen was determined at 25 °C, in two stages. First, a period of constant shear rate (100 s at $\dot{\gamma} = 1 \text{ s}^{-1}$) was used in order to supersede any residual stress due to loading and to distribute the specimen evenly between the cone and plate; the apparent viscosity at this shear rate (η_1) was evaluated by averaging the data over the final 30 s. Second, the relaxation behavior was characterized from a series of oscillatory measurements (at frequencies of 25–0.1 Hz, equivalent to angular frequencies of $\omega = 157$ to 0.63 rad s^{-1}).

As reported previously,²¹ over the frequency range used, both the elastic and viscous moduli (G' and G'') of individual silk feedstock specimens could be fitted well using binary expressions based on the Maxwellian “springs and dashpots” model:^{32–34}

$$G'(\omega) = \sum_{i=3}^4 g_i \left(\frac{\omega^2 \tau_i^2}{1 + \omega^2 \tau_i^2} \right) \quad (1a)$$

$$G''(\omega) = \sum_{i=3}^4 g_i \left(\frac{\omega \tau_i}{1 + \omega^2 \tau_i^2} \right) \quad (1b)$$

where g_i combines the modulus term and the weighting (i.e. $g_i = p_i G_i$). Hence, g_i and τ_i for the relaxation modes were evaluated by simultaneously fitting these equations to the G' and G'' data, using the “Solver” routine in Excel (Microsoft Office) software.

It should also be noted that, in addition to the modes revealed by oscillatory measurements, “quasi-static” stress relaxation in the previous work²¹ revealed two slower modes with relaxation time constants of approximately 3 and 55 s. These were designated modes 1 and 2. Subsequently, the faster modes observed in the oscillatory measurements were designated 3 and 4. For consistency, those designation are used in the present work, even though the two slowest modes are not investigated here.

For comparison, similar rheological measurements were also performed on aqueous solutions of poly(ethylene-oxide) (PEO, approximate molecular weight 600 kDa) and hydroxypropyl-methyl-cellulose (HPMC). These materials were purchased from Acros Organics BVBA, Belgium, and used as supplied. Solutions of each polymer were prepared by dissolving suitable quantities in distilled water, with gentle heating and stirring by hand; any entrained air bubbles were allowed to escape before the solutions were used. The concentrations were adjusted until the shear viscosities were comparable to those exhibited by silk feedstock specimens, then determined gravimetrically. Thus, it was found that solutions of 14.5% w/w PEO gave $\eta_1 = 630 \text{ Pa}\cdot\text{s}$, while 8.4% w/w HPMC gave $\eta_1 = 730 \text{ Pa}\cdot\text{s}$ at 25 °C.

RESULTS

Typical examples of shear viscosity data are presented in Figure 1a, demonstrating the considerable variability observed with

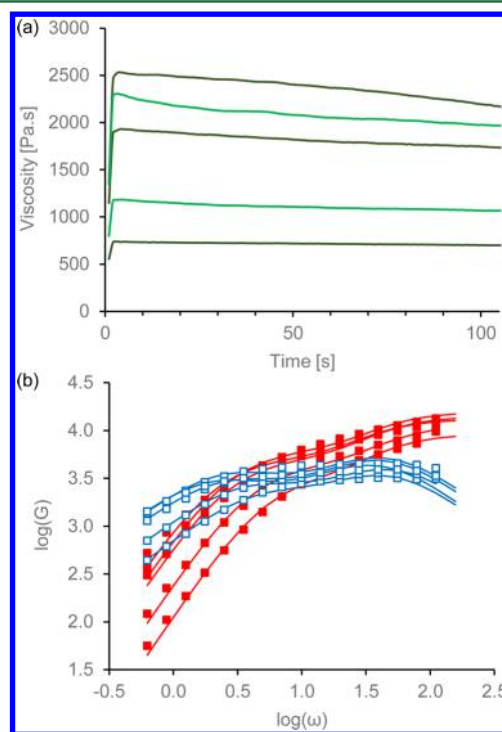


Figure 1. Examples of rheological measurements showing typical variation between five silk feedstock specimens: (a) shear flow measurements at $\dot{\gamma} = 1 \text{ s}^{-1}$, indicating measured viscosity (η_1) between 706 and 2242 Pa·s; (b) corresponding oscillatory data (G' and G'' shown as discrete symbols) with the best fits using the binary model described by eq 1 (shown as continuous lines).

native silk feedstock specimens. Indeed, these exemplars (spanning $\eta_1 = 706$ – $2242 \text{ Pa}\cdot\text{s}$) were well within the range ($\eta_1 = 418$ – $3304 \text{ Pa}\cdot\text{s}$) reported previously.²¹ In addition to the variation between specimens, it was also noted that the viscosities appeared to peak shortly (<6 s) after the start of each experiment, followed by a gradual decline over the remainder of the measurements. Similar behavior occurred with all the

specimens used and was previously ascribed to “stress overshoot”, a nonlinear effect due to the response of polymers to the sudden onset of flow.^{32–34}

The corresponding oscillatory data for these specimens are shown in Figure 1b, as plots of elastic and viscous moduli against frequency (as $\log G'$ and $\log G''$ vs $\log \omega$). In all cases, G' exceeded G'' at high frequencies, with a crossover to G'' dominating at low frequencies. This was consistent with the samples behaving as viscoelastic liquids. Nevertheless, considerable differences in the positions of the curves were observed between the specimens over the frequency range used. Hence, for measurements at $\omega = 0.63 \text{ rad s}^{-1}$ (corresponding to 0.1 Hz), the values of G' for these specimens ranged from 56 to 520 Pa, while the values of G'' ranged from 157 to 1355 Pa.

Overall, good correlations were found between the data measured in steady shear and oscillatory modes, as demonstrated in Figure 2. Values of G'' appeared to increase linearly

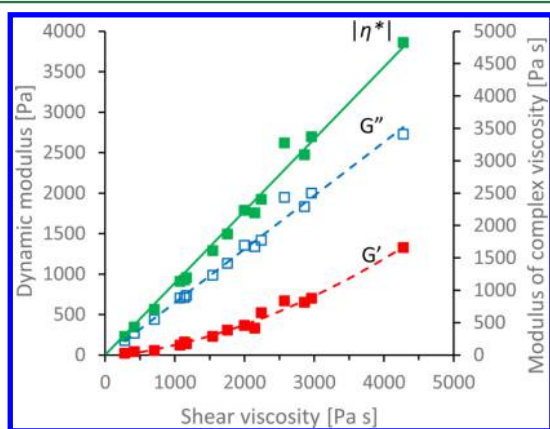


Figure 2. Relations between shear viscosity and oscillatory data (G' , G'' and $|\eta^*|$), measured at $\omega = 0.63 \text{ rad s}^{-1}$, corresponding to 0.1 Hz).

with η_1 , while G' followed a curved path, proportional to η_1^2 . The differences in rheology appeared to affect the plots of both dynamic moduli similarly; hence, higher values of G' generally corresponded to higher values of G'' . The modulus of the complex viscosity was calculated using^{32–34}

$$|\eta^*(\omega)| = \frac{\sqrt{G'^2(\omega) + G''^2(\omega)}}{\omega} \quad (2)$$

For oscillatory measurements at sufficiently low frequencies, it is expected that $|\eta^*|$ should tend toward η_0 . In line with this expectation and previous results,²¹ values of $|\eta^*|$ from the oscillatory data at $\omega = 0.63 \text{ rad s}^{-1}$ agreed closely with η_1 measured in constant shear. The slope of the trend line was found to be 1.11, which is consistent with a small amount of shear thinning at 1 s^{-1} . Moreover, the good agreement between the results from steady shear and oscillatory measurements argued against possible errors due to flow instabilities or “wall-slip” in these experiments.

Crossover Frequency and Modulus. The location of the crossover in oscillatory data (where $G' = G''$) is often regarded as the boundary between solid-like and liquid-like behavior. For measurements at frequencies higher than the crossover frequency ($\omega > \omega_X$), the material is unable to relax sufficiently quickly within the time scale of the applied oscillations and exhibits significant elastic behavior, with the storage modulus exceeding the loss modulus. Conversely, at lower frequencies,

the relaxation behavior is faster than the applied oscillations and the material exhibits viscous characteristics.

Considerable systematic variations were observed in the values of crossover modulus (G_X) and frequency, for the set of specimens used, as shown in Figure 3. It was found that G_X

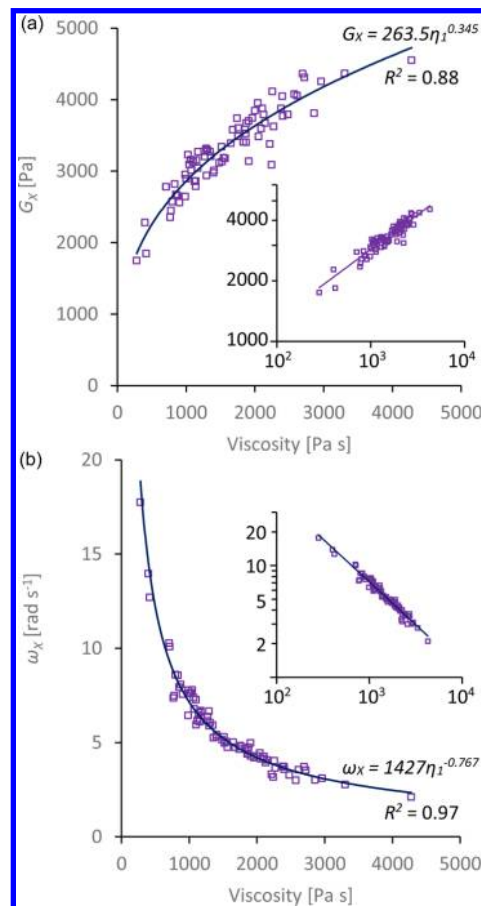


Figure 3. Relationships between (measured) viscosity and (a) crossover modulus and (b) crossover frequency. The continuous lines show the best fits and the R^2 values obtained using the equations shown. The insets present the same data on double-logarithmic axes, to emphasize the quality of the power-law fits.

increased with the viscosity (from 1749 to 4552 Pa), roughly following a power-law dependence:

$$G_X = 263.5\eta_1^{0.345} \quad (3a)$$

with a correlation coefficient of $R^2 = 0.88$. At the same time, the crossover frequency decreased with the viscosity, closely following another power-law dependence:

$$\omega_X = 1427\eta_1^{-0.767} \quad (3b)$$

with $R^2 = 0.97$. Moreover, it may be suggested that the choice of power-laws to fit these relationships appeared reasonable, as demonstrated by the double-logarithmic plots shown as insets in Figure 3. Hence, in both cases, the limitations on the correlation coefficients appear to be related more to the spread of the data, rather than the shapes of the power-law curves.

It is interesting to consider what, if any, physical significance is represented by these relations. It may be noted that, for a model system where G' and G'' can be described by single Maxwellian elements, the crossover frequency is the inverse of

the characteristic relaxation time (τ_M), while G_X is exactly half of the plateau modulus (G_N). Hence, it is expected that the zero-shear viscosity would be given by

$$\eta_0 = \frac{2G_X}{\omega_X} \quad (4a)$$

Using the relations described by eqs 3a and 3b gives

$$\begin{aligned} \eta_0 &= 2 \left(\frac{263.5}{1427} \right) \eta_1^{(0.345+0.767)} \\ &= 0.37 \eta_1^{1.1} \end{aligned} \quad (4b)$$

The small deviation in the exponent from the expected value of 1.0 may be ascribed to experimental uncertainty; hence, this further supports the choice of power-law relationships in Figure 3. The factor of 0.37 may originate from errors in this oversimplified approximation and the frequency-dependence of the complex viscosity, following the Cox–Merz rule^{32–35} in the vicinity of the crossover frequency.

Relaxation Modes from Model-Fitting Oscillatory Data. As shown in Figure 1b, the oscillatory data from individual specimens could be fitted well using the simple binary model described by eq 1. This model, which is based on a Maxwellian assembly of conceptual springs and dashpots, is able to simultaneously describe the frequency dependences of G' and G'' using only four adjustable parameters (i.e. τ_i and g_i for each mode). Empirical relations between these parameters and the shear viscosities are demonstrated in Figure 4.

As shown in Figure 4a, the modulus contributions for both modes appeared to increase with viscosity in a roughly parallel manner. Values of g_3 ranged from around 1 to 10.6 kPa, while g_4 ranged from around 4 to 14.4 kPa. Consequently, although their ranges overlapped due to changes with viscosity, the values of g_4 were consistently around 3 to 4 kPa higher than g_3 , suggesting that mode 4 made the larger contribution to the rheological behavior.

The relaxation times also increased with viscosity, as shown in Figure 4b. These changes appeared more pronounced for τ_3 (from 0.16 to 0.79 s), while τ_4 exhibited a proportionately smaller change (from 0.02 to 0.05 s). Moreover, it may be noted that there was no overlap between these ranges, with the values for τ_3 around 10 times longer than τ_4 . Consequently, the contributions to rheological behavior due to mode 4 are only expected to dominate at high frequencies, corresponding to short time scales (i.e., less than τ_4), although progressively diminishing effects will persist over longer time scales.

To put these time scales in context, examination of eq 1 shows that the contributions to G' and G'' from a specific mode are halved when the product of $\tau_i \omega = 1$. For $\tau_4 = 0.05$ s, this would occur at $\omega = 20$ rad s⁻¹ (equivalent to 3.2 Hz). The contributions decrease further at longer times, corresponding to lower frequencies, with the changes being faster for the elastic modulus, due to the squared term in the numerator. Nevertheless, 10% of the contribution to G' would still persist when $\tau_i \omega = 1/3$, which is equivalent to $\omega = 6.7$ rad s⁻¹ (or 1.07 Hz) for $\tau_4 = 0.05$ s.

Moreover, as demonstrated previously,²¹ a good estimate for the low shear-rate viscosity (before the on-set of significant shear thinning) is given by

$$\eta_0 = g_3 \tau_3 + g_4 \tau_4 \quad (5)$$

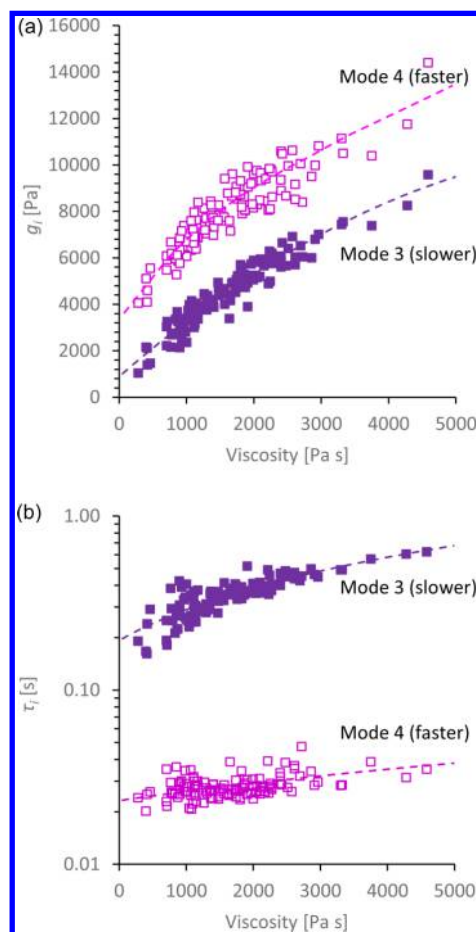


Figure 4. Relationships between (measured) viscosity and parameters extracted from oscillatory data by model fitting using eq 1: (a) modulus contributions and (b) relaxation time constants. In each case, the dashed lines serve only as guides for the eye.

In this case, the roughly 10-fold difference in relaxation times means that the low shear-rate viscosity is actually dominated by (the slower) mode 3. It was not possible to be certain whether the differences between g_3 and g_4 were due to their moduli (G_i) or abundances (p_i), as both factors contributed (i.e. $g_i = p_i G_i$). It is likely, however, that the shorter relaxation times of mode 4 imply shorter length-scales. Hence, if mode 4 involves shorter chain segments, a greater abundance than mode 3 may be expected.

The relations between the parameters describing modes 3 and 4 are demonstrated in Figure 5. There appeared to be a fairly strong correlation (with R^2 around 0.85) between g_3 and g_4 , as demonstrated in Figure 5a. This was consistent with the parallel increases in both g_3 and g_4 with viscosity that were demonstrated in Figure 4a. On the other hand, a weaker correlation (with R^2 around 0.42) was observed between the relaxation times, as demonstrated in Figure 5b. This may reflect the relatively small range exhibited by τ_4 .

Superposition of Oscillatory Data. It is well-known that rheological data for a polymer at different temperatures can often be superimposed onto a master-curve, by judicious shifting in the horizontal and vertical directions.^{32,33,36} This is termed “Time–Temperature Superposition” (TTS) and indicates “thermo-rheological simplicity”. Under ideal conditions, the shift factors are related to chain dynamics or characteristic time scales, which extends the data beyond what

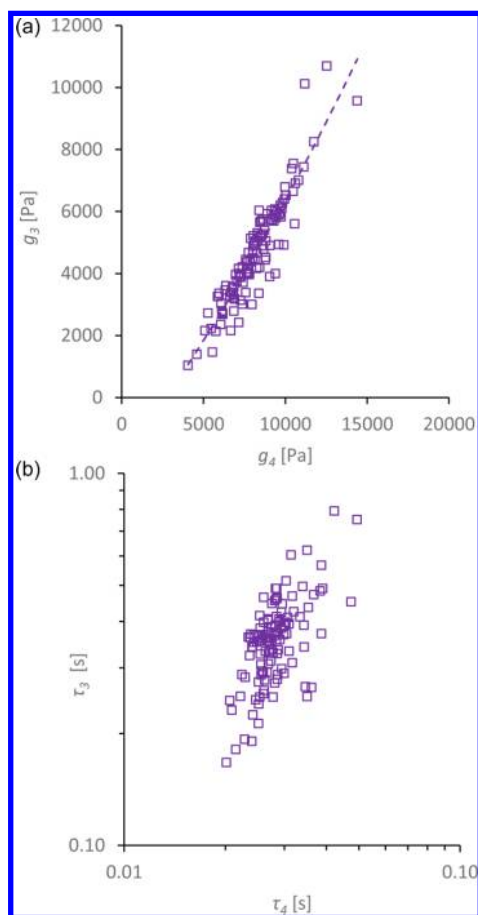


Figure 5. Correlations between relaxation modes evaluated from oscillatory data using eq 1: (a) modulus contributions and (b) relaxation time constants.

is experimentally accessible and may reveal useful information such as the activation energy of the flow process under study.^{32,36} Moreover, deviations from TTS (i.e., thermorheological complexity) can be diagnostic of more elaborate chain architectures (e.g., branching) or discontinuities in the physical behavior (e.g., due to a phase change).³⁶

The measurements on native silk feedstock specimens reported here were all performed at 25 °C, so the rheological variations observed were not attributable to temperature-dependences. Nevertheless, it was found that normalizing the oscillatory data with respect to the crossover produced a very good superposition onto a master-curve. This is demonstrated in Figure 6a, where $\log(G'/G_X)$ and $\log(G''/G_X)$ are plotted against $\log(\omega/\omega_X)$, based on the data for the five diverse specimens (with $\eta_1 = 706\text{--}2242$ Pa·s) that were originally presented in Figure 1.

In addition to producing convergence between multiple data sets, this superposition appeared to extend the angular frequency range spanned. Consequently, it was found that these results could not be fitted adequately using the model described by eq 1 with only two terms. An excellent fit was achieved by incorporating a third term (mode 5), however, as demonstrated in Figure 6a, using the parameters given in Table 1.

The parameters shown (g_i^N and ω_i^N) for the fits to the normalized and aggregated results are related to the “real” parameters by

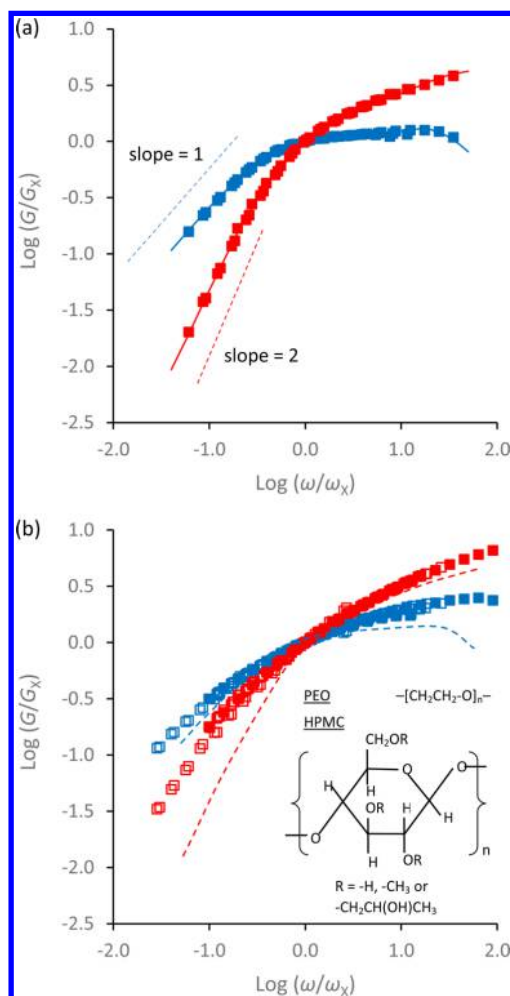


Figure 6. Oscillatory data after normalizing relative to the crossover frequencies and moduli. (a) Results from five silk feedstock specimens, for which the original data is shown in Figure 1b. The continuous lines show the best fits using the model described by eq 1 with three terms and the values of the parameters given in Table 1. The dashed lines demonstrate the slopes expected for G' and G'' toward lower frequencies. (b) Results for aqueous solutions of PEO (filled symbols) and HPMC (open symbols). The chemical structures of these polymers are shown on the graph. For ease of comparison, the dashed lines indicate the best fits through the results for the silk feedstock specimens.

Table 1. Parameters Extracted by Fitting the Normalized and Aggregated Oscillatory Data Using a Three-Term Model Described by Equation 1

mode	g_i^N	τ_i^N
3	0.720	2.463
4	1.532	0.530
5	2.236	0.052

$$g_i^N = \frac{g_i}{G_X} \quad (6a)$$

$$\tau_i^N = \tau_i \omega_X \quad (6b)$$

Hence, it was possible to calculate the corresponding modulus contributions and time constants for the original data using the measured crossover values and the model parameters extracted from fitting the master-curve. This is

demonstrated in Table 2, where results based on normalized and aggregated data are compared with the values obtained by

Table 2. Summary of Oscillatory Results Based on Data from Selected Experiments and Average Values from over 190 Individual Measurements, Including the Data Obtained Previously^{21,a}

G_X (Pa)	ω_X (rad s ⁻¹)	mode	from normalized data		from original data	
			g_i (Pa)	τ_i (s)	g_i (Pa)	τ_i (s)
Based on Results for the Specimens Shown in Figure 1						
3090.8	3.170	3	2224.7	0.777	4989.3	0.455
		4	4736.3	0.167	8102.5	0.028
		5	6911.5	0.017		
2782.9	10.259	3	2003.1	0.240	3039.7	0.193
		4	4264.5	0.052	6082.4	0.023
		5	6223.0	0.005		
3489.2	4.828	3	2511.4	0.510	4801.9	0.365
		4	5346.8	0.110	9140.3	0.025
		5	7802.3	0.011		
3843.3	4.283	3	2766.3	0.575	5892.5	0.362
		4	5889.4	0.124	9621.8	0.024
		5	8594.2	0.012		
3011.3	6.777	3	2167.5	0.363	4152.2	0.245
		4	4614.5	0.078	7152.2	0.021
		5	6733.7	0.008		
"Typical" Behavior, Derived from Average Values						
3151.9	7.008	3	2268.6	0.351	4380.3	0.321
		4	4829.9	0.076	7301.9	0.043
		5	7048.1	0.007		

^aComparisons are shown between crossover values, modulus contributions and relaxation time constants obtained by fitting normalised data using a three-term model or by fitting a binary model to the original data.

directly fitting a binary model to individual data. Parameters describing "typical" flow behavior of native silk feedstocks are also given, based on average values from over 190 individual measurements. Note: the average values shown here are slightly different from those reported previously,²¹ due to incorporating more recent data.

In each case, it was found that the relaxation times from fitting the original data fell between those obtained using the crossover values and the parameters from fitting the master-curves. This may be ascribed to the physical limitations of the binary Maxwellian model, which should be regarded as providing only an approximation for the frequency dependencies of G' and G'' . This approximation generally appeared adequate for the limited data of a single scan; indeed, the binary model produced very close fits to the oscillatory data in Figure 1b, while individual experiments yielded too few data points to ensure reliable convergence using a model with more than two terms. The binary model appeared inadequate, however, for the greater detail provided by the normalized and aggregated results from measuring multiple specimens.

Increasing the number of points and frequency range covered, by combining several data sets into a master-curve, allowing a more reliable convergence with a three-term model. In particular, this revealed a mode with a relatively large modulus contribution and relaxation time less than 0.02 s. While this represents a more accurate picture compared with binary fits to the original data, however, it is probably still not

complete. It is expected that the relaxation modes observed here were due to chain segments considerably longer than single amino acids. Additional, higher frequency processes might be expected, corresponding to shorter length scales, including vibrations within individual amino acids. These could not be observed directly with the apparatus used here, however, and probably make only minor contributions to the behavior of the silk feedstock specimens under relatively slow flow conditions. More detailed discussions of higher frequency modes have been presented by Larson and co-workers.^{37,38} At the other extreme, examination of the plot of $\log(G''/G_X)$ toward lower frequency revealed a slope of slightly less than one, suggesting contributions from multiple modes. These are expected to include the slower processes previously revealed by quasi-static stress relaxation measurements.²¹

The existence of a master-curve implied a fixed relationship between the parameters for the different modes. To put this another way, irrespective of quantitative differences in flow behavior, the oscillatory data for the native silk feedstock specimens appeared to follow a characteristic shape. Hence, the superposition appears consistent with the correlations observed between the model parameters, as shown in Figures 4 and 5.

As a comparison, similar superposition behavior was also observed with aqueous solutions of man-made (synthetic or semisynthetic) polymers (PEO and HPMC), as shown in Figure 6b. Differences in oscillatory results associated with the shear viscosities (i.e., $\eta_1 = 55$ –1182 Pa·s for PEO and 427–2360 Pa·s for HPMC) and polymer concentration were removed by normalization. Even more surprisingly, the results for PEO and HPMC coincided closely with each other, in spite of their different molecular architectures. As shown in the inset of Figure 6b, PEO is a simple linear polymer with no side-chains (only hydrogen atoms), while HPMC is based on cyclic monomers (glucose rings) randomly substituted with methyl or hydroxypropyl ether groups. Hence, this is consistent with the observed viscoelastic behavior originating from the dynamics of larger scale structures (e.g., relatively long chain segments), rather than individual monomers or short, oligomeric sequences.

Nevertheless, the normalized oscillatory results for the PEO and HPMC specimens appeared significantly broader and flatter than for native silk feedstock specimens (i.e., the data had a different overall shape). Consequently, in order to achieve an adequate fit to these normalized PEO and HPMC data, it was necessary to incorporate at least five terms into the model described by eq 1.

DISCUSSION

Previous work²¹ showed that the flow behavior of native silk feedstock specimens could exhibit considerable variability notwithstanding using (nominally) similar specimens, obtained by (essentially) identical methods from the middle-posterior divisions of silk glands of *B. mori* silkworms that had just started pupation. Rather than being merely random, however, the present work has demonstrated high levels of correlation between the various parameters. Hence, strong relations were observed between the shear viscosity and $G'(\omega)$, $G''(\omega)$, or $\eta^*(\omega)$, measured at $\omega = 1$ rad s⁻¹ (Figure 2), the values of G_X or ω_X at the crossover (Figure 3) and the values of g_i and τ_i obtained by model fitting the oscillatory data (Figure 4).

Most remarkable, however, was the observation that oscillatory data from specimens with widely divergent flow properties could be normalized relative to their crossover, to

converge onto master-curves of $\log(G'/G_X)$ and $\log(G''/G_X)$ against $\log(\omega/\omega_X)$. This was observed both for native silk feedstock specimens (Figure 6a) and two man-made polymers (Figure 6b). No previously published reports of this phenomenon with silk proteins or other polymers could be found, so it is not known how common this behavior might be. Consequently, at present, it is not possible to assess these observations within a wider perspective. Nevertheless, by analogy with TTS, the differences in flow behavior between silk feedstock specimens may be regarded as rheologically simple. Hence, for example, changes in concentration, solvation or molecular weight may be regarded as plausible explanations, while anything that would affect the relative shapes of the oscillatory data plots can be excluded. To put this in context, notwithstanding the considerable compositional differences between PEO and HPMC, only minor differences were observed between their normalized oscillatory results. This apparent insensitivity to monomer composition is consistent with the observed flow behavior being related to the dynamics of longer chain segments.

Conversely, the differences between silk feedstock specimens cannot be ascribed to discontinuous changes, such as incipient gelation due to poor sample preparation and handling. These changes would dramatically affect the relative positions of the curves describing G' and G'' ,¹⁶ which would affect the shape of the master-curve.

The master-curves for the native silk feedstock specimens were narrower than those for PEO and HPMC, probably due to differences in molecular weight distributions. It has been demonstrated extensively that increased polydispersity broadens the relaxation spectrum of polymer melts and solutions, which may be ascribed to the effects of chain length on constraint release during reptation.^{32,33,39–46} Hence, the narrower relaxation spectrum of the normalized silk feedstock results suggests a consistently narrow molecular weight distribution compared with the man-made polymers. This is consistent with expectations that the silk feedstock specimens obtained from the middle-posterior gland section should contain predominantly fibroin with monodispersed molecular weight and relatively little other (smaller or larger) protein.

It is known that the fibroin is produced under biological control, by transcription of DNA. Initially, the protein is formed in two parts as the heavy and light (Fib-H and Fib-L) chains, with molecular weights around 391 and 28 kDa, respectively.^{30,47–49} The composition of Fib-H is dominated by -Gly-Ala-Gly-Ala-Gly-Ser- sequences, which account for 88% (molar) of the amino acids. Short sections containing heavier amino acids (mainly tyrosine) occur at roughly regular intervals along the chain and somewhat greater complexity is expected toward both chain ends (i.e., the C- and N-terminals), which contain more diverse amino acids. These precursors are conjoined by a disulfide bond between a cysteine located 20 amino acids from the carboxyl terminal of Fib-H and another at residue 172 (i.e., near the middle) of Fib-L.⁵⁰ Although this results in branching, the side chains are relatively short and the Fib-H + Fib-L dimer may be regarded as an essentially linear polymer, with a monodispersed molecular weight (M_w) of around 419 kDa.

Some variations in the amino acid sequence may occur through transcription errors (homologous unequal crossing-over or misaligned, highly repetitive gene sequences) and polymorphism.⁵⁰ The associated changes in molecular weight are expected to be relatively small (<15%), however, and not

sufficient to explain the observed sample-to-sample variations in rheology. This expectation has been supported by recent analyses of silk feedstocks using gel electrophoresis, which will be reported in more detail separately.

This leaves the question of what could have caused the considerable sample-to-sample variations in the rheology of the native silk feedstocks? In order to address this question, it is useful to summarize information regarding the larger scale structures of *B. mori* silk feedstock from other techniques. NMR has been especially useful, revealing information concerning both the secondary protein structure (i.e., the local geometry) and molecular motion at the level of the amino acids. Hence, extensive work by Asakura and co-workers^{51–54} has shown that fibroin in native silk feedstock within the silk gland adopts a predominantly random coil configuration, undergoing uniform, fast segmental motion. The chain dynamics were characterized by a broad distribution of very short correlation times (ca. 10^{-10} s), which is typical of a random coil polymer in solution. This picture of native fibroin as an intrinsically disordered protein (IDP) is corroborated by Raman^{17,55,56} and infrared (IR) spectroscopy^{57,58} although these interpretations require comparisons with other known specimens, which renders them less certain than for NMR. In particular, circumspection is advisable, since other factors may influence the amide band positions that are used to assess random coil, α -helix, or β -sheet structures.⁵⁹

Dilution from the normal gland concentration increases the rate of chain motion, as indicated by changes in nuclear relaxation times.⁵³ No corresponding changes in chemical shifts were observable, however, which argues against any significant, qualitative changes in conformation or interchain interactions. Random coil conformations were also indicated by a strong negative band around 195 nm, in circular dichroism (CD) studies of diluted or redissolved silk proteins from *B. mori* and spiders.^{60–65}

Complexation between the P25 glycoprotein and Fib-H in native silk feedstock has been suggested by Tanaka and co-workers,^{66–68} which could be expected to affect the rheology. The formation of protein clusters in dilute solutions has also been suggested on the basis of dynamic light scattering (DLS).^{61,69,70} In particular, Ochi and co-workers^{69,70} reported aggregates with hydrodynamic radius (R_H) up to 240 nm, corresponding to M_w greater than 10^7 Da, which may be consistent with the P25 complex. Those findings should be treated with caution, however, since corresponding rheological measurements⁷⁰ suggested that their silk feedstock specimens had gelled.

As pointed out by Nagarkar et al.,⁶¹ the scattering intensity is proportional to the molar mass of the solute and, hence, weighted toward larger species. Although these authors observed some aggregates (with $R_H = 50–60$ nm) in redissolved fibroin specimens, they considered the concentrations to be negligible. The majority of protein yielded M_w around 300–600 kDa, suggesting that it was molecularly dispersed.

Similar inferences can also be drawn from a small-angle neutron scattering (SANS) study of diluted native silk feedstock, by Greving et al.⁷¹ Guinier analyses of their data revealed a radius of gyration (R_G) of around 10 nm, for concentrations between 0.25 and 3.5% w/w in water. Based on a typical contour length (l) of 0.36 nm per amino acid^{72,73} and the usual expression for R_G of a freely jointed polymer chain:^{74,75}

$$R_G = \sqrt{\frac{n}{6}} l \quad (7)$$

This is consistent with a degree of polymerization (n) of 4630, which is within 20% of the chain length (5524 amino acids) for the Fib-H + Fib-L dimer, estimated from gene sequencing.⁴⁹ Hence, this also suggests that the fibroin was molecularly dispersed in the dilute aqueous solution.

Taken together, all of the above studies suggest that for intermediate length scales of *B. mori* silk fibroin feedstocks, the proteins exist primarily as random coil configurations with little significant change in conformation in response to overall concentration. It may also be noted that our control PEO is expected to adopt a random coil configuration and be molecularly dispersed in the solution used,⁷⁶ while HPMC may exhibit significant interchain interactions due to its uneven substitution pattern.^{77,78}

Returning to the present results, some differences in protein concentration may have occurred, due to the production of fibroin or the sericins, which are incorporated into the silk feedstock in the middle gland division.⁴² Nevertheless, previous work²¹ found only a weak correlation between viscosity and the protein concentration, while any associated changes in molecular weight distributions were insufficient to affect the shape of normalized oscillatory results.

One possibility is that differences in pH or ion content in the silk glands may have affected the rheology, through changes in solvation, conformation, chain size (i.e., radius of gyration, R_G) or the strength of interchain interactions. In this respect, Terry et al.²⁵ demonstrated pH-induced changes in the rheology of native silk feedstock, with gelation becoming evident ($G' > G''$ over the entire frequency range) on acidification and reversion to a viscous liquid ($G' < G''$ at low frequency) on raising the pH again. It may be noted, however, that these pH-induced changes in dynamic moduli would greatly affect the shapes of the normalized results, in contrast to the sample-to-sample variations observed in the present work, which still converged onto a consistent master curve.

Another interesting possibility is post-translational modification (PTM). It is known that proteins within biological systems are often chemically modified (e.g., glycosylated or phosphorylated) to control their movement or reactivity. In this respect, various degrees of phosphorylation have been reported among proteins within the gland contents⁷⁹ and cocoon fiber.⁸⁰ It may be noted that phosphorylation is commonly observed on serine and tyrosine, which account for around 17% (molar) of the amino acids in Fib-H. Moreover, although PTM of fibroin is likely to affect the protein solvation and coil geometry,⁸¹ these effects might not be revealed in the normalized oscillatory results. The possible role of phosphorylation is currently under investigation and will be reported elsewhere.

As a final point, the superposition of rheological data onto a master curve suggested that, in spite of quantitative differences between samples, the flow behavior exhibited a qualitative consistency. The normalized and aggregated results may be regarded as the “ground-state” of *B. mori* silk feedstocks, providing a more representative basis for future biomimetic and modeling endeavors. In this respect, one may draw a parallel with the previous suggestion by Elices and co-workers⁸² that the mechanical behavior of supercontracted spider silks represents the “ground-state”, which can be modified by further treatments.

CONCLUSIONS

Native silk feedstocks showed considerable sample-to-sample variations in both shear flow and oscillatory behavior. Rather than being purely random, however, the present work demonstrated considerable correlations between the parameters measured or obtained by model-fitting.

In spite of the sample-to-sample variations observed in oscillatory measurements of native silk feedstocks, normalization with respect to the crossover produced a remarkable superposition of the results. This extended the effective frequency range covered by the oscillatory measurements, such that a three-term model was required to successfully fit the normalized results.

Moreover, in keeping with conventional TTS, the observed superposition suggested that the differences between specimens were rheologically simple. This ruled out incipient gelation as an explanation, as this would dramatically change the shape and relative positions of the curves describing G' and G'' .

Several potential explanations for the differences between silk feedstock specimens were discussed, including PTM of the fibroin in the form of phosphorylation. Phosphorylation is commonly observed on serine and tyrosine, which constitute around 17% (molar) of the amino acids in the Fib-H chain. This has been observed previously in *B. mori* silk and may be expected to affect the protein solution characteristics, although potential effects on the rheology are currently unknown and merit further investigation.

Similar superposition behavior was also observed for HPMC and PEO solutions, although the resulting master-curves were somewhat broader than for silk feedstocks. This difference was ascribed to the molecular weight distributions, since greater polydispersity is expected to produce a broader relaxation spectrum. No previous reports of this phenomenon could be found, however, so it is not known how common it might be or what deeper significance it might represent.

AUTHOR INFORMATION

Corresponding Authors

*E-mail: petelaity@aol.com.

*E-mail: christopher.holland@sheffield.ac.uk.

Notes

The authors declare no competing financial interest.

ACKNOWLEDGMENTS

This work was funded by the EPSRC, Project Reference EP/K005693/1.

REFERENCES

- (1) Craig, C. L. *Annu. Rev. Entomol.* **1997**, *42*, 231–267.
- (2) Walker, A. A.; Holland, C.; Sutherland, T. D. *Proc. R. Soc. London, Ser. B* **2015**, *282*, 20150259.
- (3) Koh, L.-D.; Cheng, Y.; Teng, C.-P.; Khin, Y.-W.; Loh, X.-J.; Tee, S.-Y.; Low, M.; Ye, E.; Yu, H.-D.; Zhang, Y.-W.; Han, M.-Y. *Prog. Polym. Sci.* **2015**, *46*, 86–110.
- (4) Liu, X.; Zhang, K.-Q. Silk fiber: molecular formation mechanism, structure–property relationship and advanced applications. In *Oligomerization of Chemical and Biological Compounds*; Lesieur, C., Ed. InTech, 2014; <http://dx.doi.org/10.5772/57611>.
- (5) Vollrath, F.; Porter, D.; Holland, C. *MRS Bull.* **2013**, *38*, 73–80.
- (6) Brunetta, L.; Craig, C. L. *Spider Silk*; Yale University Press: New Haven, 2010.
- (7) Eisoltd, L.; Smith, A.; Scheibel, T. *Mater. Today* **2011**, *14*, 80–86.
- (8) Vollrath, F.; Knight, D. P. *Nature* **2001**, *410*, 541–548.

- (9) Collin, M. A.; Edgerly, J. S.; Hayashi, C. Y. *Zoology* **2011**, *114*, 239–246.
- (10) Sutherland, T. D.; Young, J. H.; Weisman, S.; Hayashi, C. H.; Merritt, D. J. *Annu. Rev. Entomol.* **2010**, *55*, 171–88.
- (11) Sehna, F.; Sutherland, T. *Prion* **2008**, *2*, 145–153.
- (12) Golovatch, S. I.; Kime, D. *Soil Organisms* **2009**, *81*, 565–597.
- (13) Brunhuber, B. S.; Hall, E. *Zool. J. Linn. Soc. London* **1970**, *49*, 49–59.
- (14) Knight, D. P.; Knight, M. M.; Vollrath, F. *Int. J. Biol. Macromol.* **2000**, *27*, 205–210.
- (15) Downes, A. M.; Sharry, L. F. *Aust. J. Biol. Sci.* **1971**, *24*, 117–130.
- (16) Holland, C.; Urbach, J. S.; Blair, D. L. *Soft Matter* **2012**, *8*, 2590–2594.
- (17) Magoshi, J.; Magoshi, Y.; Nakamura, S. *Polym. Comm.* **1985**, *26*, 309–311.
- (18) Moncrief, R. W. *Man-Made Fibres*; Newnes-Butterworths: London, 1975.
- (19) Zhang, D., Ed. *Advances in Filament Yarn Spinning of Textiles and Polymers*; Woodhead Publishing Ltd.: Cambridge, 2014.
- (20) Holland, C.; Vollrath, F.; Ryan, A. J.; Mykhaylyk, O. O. *Adv. Mater.* **2012**, *24*, 105–109.
- (21) Laity, P. R.; Gilks, S. E.; Holland, C. *Polymer* **2015**, *67*, 28–39.
- (22) Holland, C.; Porter, D.; Vollrath, F. *Biopolymers* **2012**, *97*, 362–367.
- (23) Holland, C.; Terry, A. E.; Porter, D.; Vollrath, F. *Polymer* **2007**, *48*, 3388–3392.
- (24) Holland, C.; Terry, A. E.; Porter, D.; Vollrath, F. *Nat. Mater.* **2006**, *5*, 870–874.
- (25) Terry, A. E.; Knight, D. P.; Porter, D.; Vollrath, F. *Biomacromolecules* **2004**, *5*, 768–772.
- (26) Jin, Y.; Hang, Y.; Juo, J.; Zhang, Y.; Shao, H.; Hu, X. *Int. J. Biol. Macromol.* **2013**, *62*, 162–166.
- (27) Moriya, M.; Roschztardt, F.; Nakahara, Y.; Saito, H.; Masabuchi, Y.; Asakura, T. *Biomacromolecules* **2009**, *10*, 929–935.
- (28) Kojić, N.; Bico, J.; Clasen, C.; McKinley, G. H. *J. Exp. Biol.* **2006**, *209*, 4355–4362.
- (29) Chen, X.; Knight, D. P.; Vollrath, F. *Biomacromolecules* **2002**, *3*, 644–648.
- (30) Manning, R. F.; Gage, L. P. *J. Biol. Chem.* **1980**, *255*, 9451–9457.
- (31) Craig, C. L.; Riekel, C. *Comp. Biochem. Physiol., Part B: Biochem. Mol. Biol.* **2002**, *133*, 493–507.
- (32) Ferry, J. D. *Viscoelastic Properties of Polymers*, 3rd ed.; John Wiley & Sons Inc.: New York, 1980.
- (33) Larson, R. G. *The Structure and Rheology of Complex Fluids*; Oxford Univ. Press: New York, 1999.
- (34) Goodwin, J. W.; Hughes, R. W. *Rheology for Chemists: An Introduction*; Royal Society of Chemistry: Cambridge, 2008.
- (35) Mead, D. W. *Rheol. Acta* **2011**, *50*, 837–866.
- (36) Dealy, J.; Plazek, D. *Rheol. Bull.* **2009**, *78*, 16–31.
- (37) Dalal, I. S.; Larson, R. G. *Macromolecules* **2013**, *46*, 1981–1992.
- (38) Larson, R. G. *Macromolecules* **2004**, *37*, 5110–5114.
- (39) Ye, X.; Sridhar, T. *Macromolecules* **2005**, *38*, 3442–3449.
- (40) Watanabe, H. *Prog. Polym. Sci.* **1999**, *24*, 1253–1403.
- (41) Carrot, C.; Revenu, P.; Guillet, J. J. *Appl. Polym. Sci.* **1996**, *61*, 1887–1897.
- (42) Cassagnau, P.; Montfort, J. P.; Monge, P. *Rheol. Acta* **1993**, *32*, 156–167.
- (43) Montfort, J. P.; Marin, G.; Monge, P. *Macromolecules* **1986**, *19*, 1979–1988.
- (44) Montfort, J. P.; Marin, G.; Monge, P. *Macromolecules* **1986**, *19*, 393–399.
- (45) Montfort, J. P.; Marin, G.; Monge, P. *Macromolecules* **1984**, *17*, 1551–1560.
- (46) Masuda, T.; Kitagawa, K.; Inoue, T.; Onogi, S. *Macromolecules* **1970**, *3*, 116–125.
- (47) Gamo, T.; Inokuchi, T.; Laufer, H. *Insect Biochem.* **1977**, *7*, 285–295.
- (48) Zhou, C.-Z.; Confalonieri, F.; Medina, N.; Zivanovic, Y.; Esnault, C.; Yang, T.; Jacquet, M.; Janin, J.; Duguet, M.; Perasso, R.; Li, Z.-G. *Nucl. Acids Res.* **2000**, *28*, 2413–2419.
- (49) Gene and corresponding amino-acid sequences for silk proteins of *B. mori* and several wild species are available on-line, at GenBank: <http://www.ncbi.nlm.nih.gov/genbank/>.
- (50) Tanaka, K.; Kajiyama, N.; Ishikura, K.; Waga, S.; Kikuchi, A.; Ohtomo, K.; Takagi, T.; Mizuno, S. *Biochim. Biophys. Acta, Protein Struct. Mol. Enzymol.* **1999**, *1432*, 92–103.
- (51) Asakura, T.; Okushita, K.; Williamson, M. P. *Macromolecules* **2015**, *48*, 2345–2357.
- (52) Zhao, C.; Asakura, T. *Prog. Nucl. Magn. Reson. Spectrosc.* **2001**, *39*, 301–352.
- (53) Asakura, T.; Watanabe, Y.; Uchida, A.; Minagawa, H. *Macromolecules* **1984**, *17*, 1075–1081.
- (54) Asakura, T.; Suzuki, H.; Watanabe, Y. *Macromolecules* **1983**, *16*, 1024–1026.
- (55) Lefèvre, T.; Paquet-Mercier, F.; Rioux-Dubé, J.-F.; Pézolet, M. *Biopolymers* **2012**, *97*, 322–336.
- (56) Zheng, S.; Li, G.; Yao, W.; Yu, T. *Appl. Spectrosc.* **1989**, *43*, 1269–1272.
- (57) Percot, A.; Colomban, P.; Paris, C.; Dinh, H.-M.; Wojcieszak, M.; Mauchamp, B. *Vibr. Vib. Spectrosc.* **2014**, *73*, 79–89.
- (58) Boulet-Audet, M.; Terry, E. A.; Vollrath, F.; Holland, C. *Acta Biomater.* **2014**, *10*, 776–784.
- (59) Surewicz, W. K.; Mantsch, H. H.; Chapman, D. *Biochemistry* **1993**, *32*, 389–394.
- (60) Yao, T.; Jiang, T.; Pan, D.; Xu, Z.-X.; Zhou, P. *RSC Adv.* **2014**, *4*, 40273–40280.
- (61) Nagarkar, S.; Nicolai, T.; Chassenieux, C.; Lele, A. *Phys. Chem. Chem. Phys.* **2010**, *12*, 3834–3844.
- (62) Dicko, C.; Porter, D.; Bond, J.; Kenney, J. M.; Vollrath, F. *Biomacromolecules* **2008**, *9*, 216–221.
- (63) Dicko, C.; Kenney, J. M.; Knight, D.; Vollrath, F. *Biochemistry* **2004**, *43*, 14080–14087.
- (64) Dicko, C.; Knight, D.; Kenney, J. M.; Vollrath, F. *Biomacromolecules* **2004**, *5*, 758–767.
- (65) Iizuka, E.; Yang, J. T. *Biochemistry* **1968**, *7*, 2218–2228.
- (66) Inoue, S.; Tanaka, K.; Arisaka, F.; Kimura, S.; Ohtomo, K.; Mizuno, S. *J. Biol. Chem.* **2000**, *275*, 40517–40528.
- (67) Tanaka, K.; Inoue, S.; Mizuno, S. *Insect Biochem. Mol. Biol.* **1999**, *29*, 269–276.
- (68) Tanaka, K.; Mori, K.; Mizuno, S. *Biochemistry* **1993**, *114*, 1–4.
- (69) Hossain, K. S.; Ochi, A.; Ooyama, E.; Magoshi, J.; Nemoto, N. *Biomacromolecules* **2003**, *4*, 350–359.
- (70) Ochi, A.; Hossain, K. S.; Magoshi, J.; Nemoto, N. *Biomacromolecules* **2002**, *3*, 1187–1196.
- (71) Greving, I.; Dicko, C.; Terry, A.; Callow, P.; Vollrath, F. *Soft Matter* **2010**, *6*, 4389–4395.
- (72) Ainaverapu, S. R. K.; Brujić, J.; Huang, H. H.; Wiita, A. P.; Liu, H.; Li, L.; Walther, K. A.; Carrion-Vazques, M.; Li, H.; Fernandez, J. M. *Biophys. J.* **2007**, *92*, 225–233.
- (73) Pauling, L.; Corey, R. B. *Proc. Natl. Acad. Sci. U. S. A.* **1951**, *37*, 251–256.
- (74) Gedde, U. W. *Polymer Physics*; Kluwer Academic Publishers: Dordrecht, 1999.
- (75) Cowie, J. M. G. *Polymers: Chemistry and Physics of Modern Materials*; Blackie Academic and Professional: London, 1991.
- (76) Hezaveh, S.; Samanta, S.; Milano, G.; Roccatano, D. J. *J. Chem. Phys.* **2012**, *136*, 124901.
- (77) Viridén, A.; Wittgren, B.; Andersson, T.; Abrahamsén-Alami, S.; Larsson, A. *Biomacromolecules* **2009**, *10*, 522–529.
- (78) Haque, A.; Richardson, R. K.; Morris, E. R.; Gidley, M. J.; Caswell, D. C. *Carbohydr. Carbohydr. Polym.* **1993**, *22*, 175–186.
- (79) Zhang, P.; Aso, Y.; Yamamoto, K.; Banno, Y.; Wang, Y.; Tsuchida, K.; Kawaguchi, Y.; Fujii, H. *Proteomics* **2006**, *6*, 2586–2599.
- (80) Chen, W.-Q.; Prielwalder, H.; John, J. P. P.; Lubec, G. *Proteomics* **2010**, *10*, 369–379.

(81) Winkler, S.; Wilson, D.; Kaplan, D. L. *Biochemistry* **2000**, *39*, 12739–12746.

(82) Elices, M.; Plaza, G. R.; Pérez-Rigueiro, J.; Guinea, G. V. *J. Mech. Behav. Biomed.* **2011**, *4*, 658–669.